High spatial resolution sensing by using stepped pump light and its experimental validation

Tong Guo (郭 彤)[1*] and Ningsheng Yu (虞宁生)[2]

[1]*Structural Health Monitoring Institute, Southeast University, Nanjing 210096, China*

[2]*Nanjing COECOM Light and Electronic Equipment Co., Ltd., Nanjing 210018, China*

[*]*E-mail: guotong77@gmail.com*

Received August 25, 2008

The spatial resolution of conventional distributed fiber optic sensors is 1 m at best, which is inadequate to locate the damage precisely. We adopt an improved sensing technique based on the Brillouin optical time-domain analysis (BOTDA). The stepped pump light is input to stimulate the phonon so that the spatial resolution can be increased to centimeter order and the strain accuracy of 25 micro-strains is obtained. The feasibility of this sensing technique is demonstrated through strain measurement of three concrete box-girders in bending. Experimental results show that the improved BOTDA measurement can provide a comprehensive description on the strain distribution of steel rebar or concrete. Compared with the conventional strain gauges, the improved BOTDA measurement is more stable. By virtue of higher spatial resolution and better measurement accuracy, it has become possible to perform crack detection and localization for concrete structures.

OCIS codes: 060.2370, 120.0280, 060.2300.

doi: 10.3788/COL20090706.0465.

Distributed optical fiber sensors based on Brillouin scattering have attracted much attention in the past years due to their notable advantages[1,2]. They are free from electromagnetic interference and corrosion; meanwhile, they can provide continuous strain and temperature measurements. Some primary applications have been made in monitoring large structures such as dams, tunnels, pipelines, oil wells, bridges, landslide, etc. The Brillouin-based sensing techniques can generally be classified into two types, namely the spontaneous-scattering-based type and the stimulated-scattering-based type. Brillouin optical time-domain reflectometry (BOTDR)[3,4] belongs to the former, and Brillouin optical time-domain analysis (BOTDA)[5−8] is included in the latter. A BOTDR system enables us to perform measurements by accessing only one end of the sensing fiber. This is an advantage of the BOTDR system over the BOTDA system because we have to access both ends of the sensing fiber when using the BOTDA system. However, the spatial resolution of the conventional BOTDR system is 1 m at best, although some progress has been made toward further enhancement of the BOTDA system. In order to meet the need of damage diagnosis, especially for crack monitoring of civil structures, sensors with centimeter order resolution are needed. Because the spatial resolution is proportional to the pump light width, theoretically we can decrease the pump light width to get higher resolution. Unfortunately, as it takes approximately up to 28 ns to stimulate the phonon waves in the fiber, the consequence of small width of the pump light is a decrease and distortion in the stimulated Brillouin scattering (SBS) gain[9].

In this letter, the existing BOTDA system is improved by using a stepped pump light. The improved system, developed by the Neubrex Co., Ltd., can stimulate the phonon to move prior to the arrival of probe light, so that the spatial resolution can be increased up to centimeter order and a strain resolution of $\pm 0.0025\%$ is obtained. The schematic diagram of this improved BOTDA operation is shown in Fig. 1. The stepped pump light, as shown in Fig. 1, can be described by

$$A_{\rm P}(t) = \begin{cases} C_{\rm P}, & 0 \le t \le T_{\rm pre} - T_{\rm D} \\ A_{\rm p} + C_{\rm p}, & T_{\rm pre} - T_{\rm D} \le t \le T_{\rm pre} \\ 0, & \text{other cases} \end{cases}, \quad (1)$$

where $A_{\rm p}$ and $C_{\rm p}$ stand for the amplitudes of the pre-pump light and the pump light, t stands for time, $T_{\rm D}$ denotes the pump light duration, $T_{\rm pre}$ stands for the pre-pump duration.

According to the perturbation theory, the intensity of the probe light is[9]

$$E_{\rm CW}(0,t) = A_{\rm CW}[1 + \beta H(t,\Omega)], \quad (2)$$

where $A_{\rm CW}$ is the amplitude of the probe light, β stands for the perturbation parameter, Ω is the frequency of phonon, that is, the difference between frequencies of pump light and probe light. $H(t,\Omega)$ stands for the SBS, the double integration of the

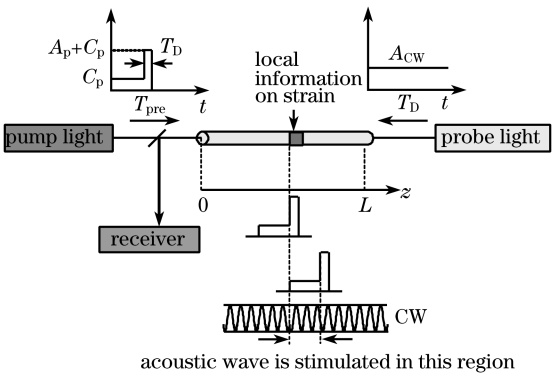

Fig. 1. Schematic diagram of the improved BOTDA operation.

pump profile, and can be described by

$$H(t,\Omega) = \int_0^L A\left(t-\frac{2z}{v_g}\right)\int_0^\infty h(z,s) \times A\left(t-s-\frac{2z}{v_g}\right)\mathrm{d}s\mathrm{d}z, \quad (3)$$

where A is the amplitude of pump light consisitng of A_p and C_p, v_g is the light speed, and $h(z,s)$ expresses the phonon behavior:

$$h(z,s) = \Gamma \mathrm{e}^{-[\Gamma+\mathrm{i}(\Omega_\mathrm{B}(z)-\Omega)]s}. \quad (4)$$

In Eq. (3), L is the length of fiber, and $\Omega_\mathrm{B}(z)$ in Eq. (4) is the Brillouin center frequency. Furthermore, $\Gamma = \Gamma_\mathrm{B}/2$, and Γ_B is the full-width at half-maximum (FWHM) of Brillouin spectrum. The power of Brillouin gain spectrum (BGS)[10] can be expressed as

$$V(t,\Omega) = \frac{1}{2}\beta A_\mathrm{CW}^2 H(t,\Omega) + c.c. \quad (5)$$

When the input pump light is a stepped one, as shown in Eq. (1), $H(t,\Omega)$ can be split into four terms[9], namely,

$$H(t,\Omega) = H_1(t,\Omega) + H_2(t,\Omega) + H_3(t,\Omega) + H_4(t,\Omega), \quad (6)$$

$$H_1(t,\Omega) = A_\mathrm{P}^2 \int_{v_g(t-T_\mathrm{pre})/2}^{v_g(t-T_\mathrm{pre}+T_\mathrm{D})/2} \times \int_0^{t-T_\mathrm{pre}+T_\mathrm{D}-2z/v_g} h(z,s)\mathrm{d}s\mathrm{d}z, \quad (7)$$

$$H_2(t,\Omega) = A_\mathrm{P}C_\mathrm{P} \int_{v_g(t-T_\mathrm{pre})/2}^{v_g(t-T_\mathrm{pre}+T_\mathrm{D})/2} \times \int_0^{t-2z/v_g} h(z,s)\mathrm{d}s\mathrm{d}z, \quad (8)$$

$$H_3(t,\Omega) = A_\mathrm{P}C_\mathrm{P} \int_{v_g(t-T_\mathrm{pre})/2}^{v_g(t-T_\mathrm{pre}+T_\mathrm{D})/2} \times \int_0^{t-T_\mathrm{pre}+T_\mathrm{D}-2z/v_g} h(z,s)\mathrm{d}s\mathrm{d}z, \quad (9)$$

$$H_4(t,\Omega) = C_\mathrm{P}^2 \int_{v_g(t-T_\mathrm{pre})/2}^{v_g t/2} \int_0^{t-2z/v_g} \times h(z,s)\mathrm{d}s\mathrm{d}z. \quad (10)$$

The term H_1 represents the pump light, which is the conventional term in the BOTDA, and it has high spatial resolution and wide spectrum span. The term H_2 stands for the interaction of pump with pre-pump, and it has high spatial resolution and narrow spectrum span. According to the research of Bao *et al.*[11], the spectrum of H_2 can have the same FWHM as continuous wave (CW). H_3 stands for the interaction of pre-pump and pump, and it contains vibration noise and complicated contents. The term H_4, representing the pre-pump light, has a direct link with the total length of fiber and has low spatial resolution and narrow spectrum span, therefore, it is not suitable for strain measurement.

Input the pre-pump light and ensure that T_pre is of finite duration (e.g., $10-28$ ns). In such case, H_3 will have the same value as H_1, while H_4 is limited to the length of pump light. As long as the optical fiber is longer than $t_\mathrm{D}\cdot v_g$, BGS does not decrease. The contribution of H_2 makes a narrow peak to appear on the BGS, as shown in Fig. 2, which enables higher spatial resolution and better strain measurement precision.

In order to investigate the feasibility of this improved BOTDA system, the strain measurement of three reinforced concrete (RC) box-girders in bending was conducted, as shown in Fig. 3. These girders are the scaled models of those used widely in highway bridges. Figure 4 shows the layout of sensors on the box-girders. The fibers were mainly fixed longitudinally on the girders. Several conventional strain gauges were also installed in the mid-span section to compare with the performance of the fiber optical sensors.

The optical fibers used in this test were the tight buffered single-mode ones with a diameter of 900 μm. The tight buffer was made of nylon that can bear a maximum tensile load of 4.5 N (corresponding to the

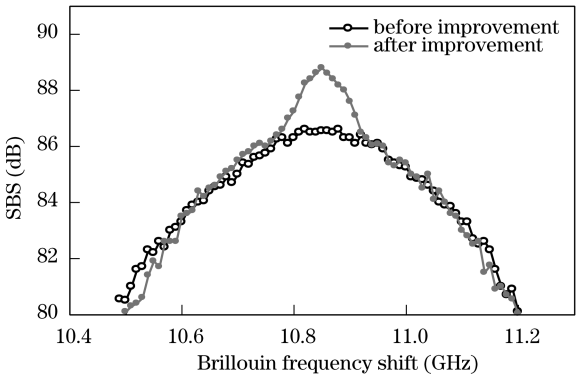

Fig. 2. Comparison of the SBS spectra.

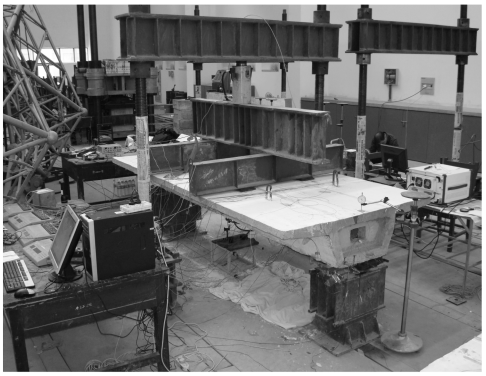

Fig. 3. Strain measurement of the RC box-girder in bending.

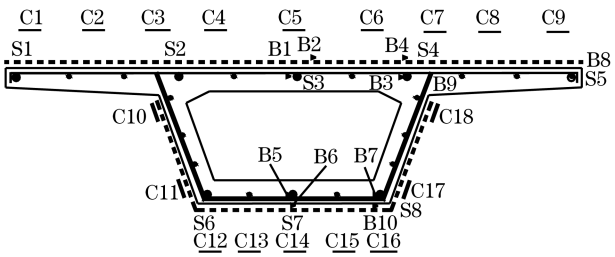

Fig. 4. Layout of sensors in the mid-span section of the girders. C: strain gauge for concrete; S: strain gauge for rebar; B: BOTDA optical fiber sensor. The gauges in girders 2 and 3 are identified by putting "J" and "G" in front of their serial numbers.

0.3% fiber strain), and the minimum bending radius of the fiber was 30 mm. The optical fibers were fixed onto the concrete surface or steel rebars separately by epoxy resin adhesive, and the separately fixed optical fibers were finally connected into a loop, after procedures including end peeling, dedusting, end cutting, alignment, and melting, etc. Finally the optical fiber loop was connected to the analyzer (NBX-6000) through the FC/APC connectors.

Because the Brillouin frequency shift is proportional to the strain or temperature[7], the strain $\varepsilon(x)$ of each point along the optical fiber can be calculated by

$$\varepsilon(x) = \frac{(\Omega_{\rm B}(x) - \Omega_{\rm B}(0))}{C}, \tag{11}$$

where $\Omega_{\rm B}(x)$ denotes the center frequency, which can be fitted based on the BGS, as shown in Fig. 5; $\Omega_{\rm B}(0)$ stands for the zero frequency shift, and here it takes 10.826 GHz; the value of constant C is determined by the kind of optical fiber, and for the tight buffered single-mode fiber in this study, it takes 0.04970 MHz/$\mu\varepsilon$. Therefore, a frequency shift of about 50 MHz represents the strain value of 1000 $\mu\varepsilon$.

For the single-mode optical fiber, the Brillouin frequency is usually shifted from 10.8 to 10.9 GHz. In this test, the frequency scanning range was set from 10.7 to 11.1 GHz. In order to measure the expected high strain values, high spatial resolution is usually required. However, this will sometimes result in the decrease of the signal-to-noise ratio (SNR) and thus the available distance range becomes shorter. In the test, the fiber loop was no more than 100 m, and the spatial sampling intervals were set to 5 cm. For the frequency scanning, we used 81 counts (number of steps) with a step length of 5 MHz. The probe power and the pump power were +0 and +25 dBm, respectively (if the SNR is low, the value of probe power needs to be set to a value greater than 0 dBm). The duration of the pump light was 28 ns.

Figure 6 shows the strain distributions of the two longitudinal rebars in the bottom plate of the girder 1. As can be seen, the strains are generally trapezoidally distributed, which is consistent with theoretical analysis. When the applied load was up to 340 kN, several peaks appeared on the strain curve, and this was because of the widely propagated cracks that made the rebar yielding. However, at that time the rebar strains measured by the conventional strain gauges had not reached the yielding value. An explanation to this phenomenon is that the strains obtained by the strain gauges are only local strains, which are inadequate to cover the maximum strain of the rebar. This phenomenon also demonstrates the superiority of the distributed strain measurement.

Figure 7 gives the tensile strain distributions on the bottom plate of the girder 2, and the observed cracks are given above these strain curves. We can see that the peaks on the strain curves are consistent with the position of the observed cracks. Therefore, the increase in spatial resolution by virtue of the improved BOTDA has made it possible to perform crack monitoring and detection for concrete structures.

When measuring the tensile strains of the concrete girders, the optical fiber sensors also show the superiority over the conventional strain gauges, as shown in

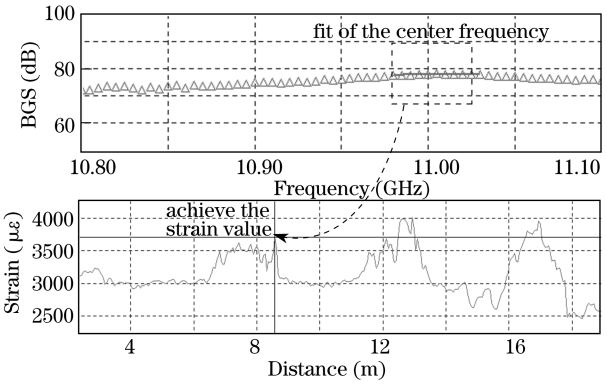

Fig. 5. Fit of the center frequency from the BGS to achieve the strain value.

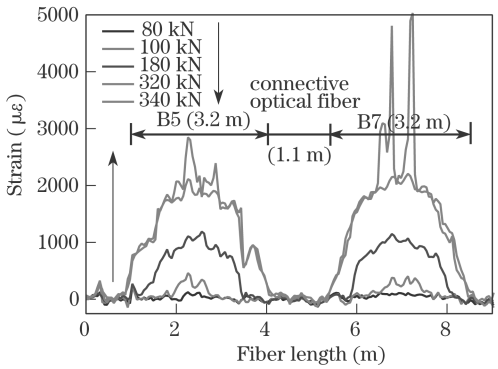

Fig. 6. Rebar strain distributions under various loads.

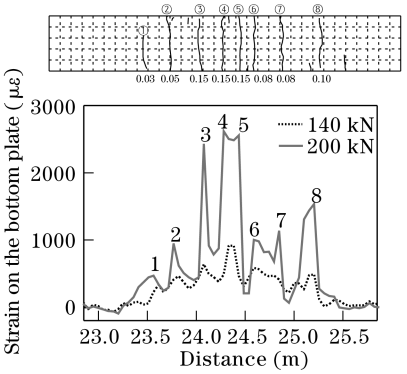

Fig. 7. Longitudinal strain distribution on the surface of bottom plate (the strain data of the sensor GB6). $1-8$ are the serial numbers of cracks, the data under the cracks stand for crack widths in millimeters.

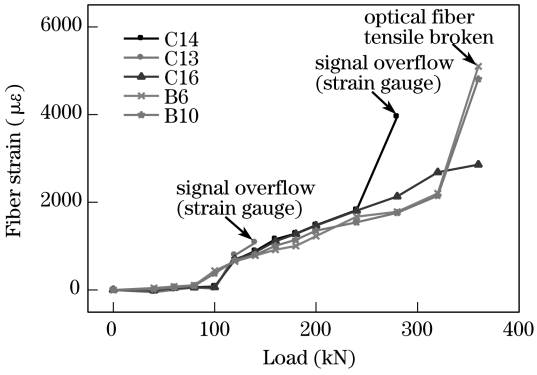

Fig. 8. Comparison of optical fiber sensor and strain gauges in the tensile strain measurement.

Fig. 8. Because cracks initiated under relatively small load levels, which affected the stability of the strain gauges, most strain gauges in the tensile region overflowed under the small loads. For example, signal of the conventional gauge C13 overflowed under the load of 160 kN, C14 and C16 overflowed under the load of 320 and 380 kN, respectively, while the strain measurement using the optical fibers was rather stable before the tensile failure under the load of 360 kN.

In summary, higher spatial resolution and better accuracy are achieved by using the elaborately designed stepped pump light scheme. This ongoing research, requiring further improvements in both measuring and solution techniques, demonstrates the capabilities of the proposed methodology and clearly shows that it is promising in damage diagnosis and crack monitoring for large concrete structures.

This work was supported by the National Natural Science Foundation of China (Nos. 50725828 and 50608017) and the Sustentation Fund for Young Teachers of Southeast University.

References

1. X. Bao, M. DeMerchant, A. Brown, and T. Bremner, J. Lightwave Technol. **19,** 1698 (2001).
2. H. Izumita, T. Horiguchi, and T. Kurashima, in *Proceedings of 12th International Conference on Optical Fiber Sensors* 316 (1997).
3. K. Shimizu, T. Horiguchi, and Y. Koyamada, Opt. Lett. **20,** 507 (1995).
4. H. Ohno, H. Naruse, M. Kihara, and A. Shimada, Opt. Fiber Technol. **7,** 45 (2001).
5. Z. Zhou, J. He, K. Yan, and J. Ou, Opt. Eng. **47,** 014401 (2008).
6. D. Garus, T. Gogolla, K. Krebber, and F. Schliep, J. Lightwave Technol. **15,** 654 (1997).
7. I.-B. Kwon, S.-J. Baik, K. Im, and J.-W. Yu, Sensors and Actuators A **101,** 77 (2002).
8. M. Song and B. Zhuang, Acta Opt. Sin. (in Chinese) **27,** 711 (2007).
9. K. Kishida, C. Li, S. Lin, and K. Nishiguchi, Technical Report of IEICE (in Japanese) OFT 2000-47 15 (2004).
10. M. Niklès, L. Thévenaz, and P. A. Robert, J. Lightwave Technol. **15,** 1842 (1997).
11. X. Bao, A. Brown, M. DeMerchant, and J. Smith, Opt. Lett. **24,** 510 (1999).